JOURNAL OF MATERIALS SCIENCE 13 (1978) 2487–2496

Growth morphology of the tetragonal phase in partially stabilized zirconia

R. H. J. HANNINK
CSIRO, Division of Materials Science, P.O. Box 4331, Melbourne 3001, Victoria, Australia

The zirconia-rich, metastable tetragonal phase in partially stabilized zirconia–magnesia, zirconia–calcia and zirconia–yttria is examined using electron microscopy and electron and X-ray diffraction. The tetragonal phase precipitate distribution is that normally associated with homogeneously nucleated coherent precipitation. An attempt is made to explain the growth morphology of the tetragonal phase in terms of the cubic–tetragonal lattice parameter mismatch. It is found that the tetragonal phase is retained at room temperature provided coherency with the cubic matrix is retained. Once coherency is lost, due to growth strains or mechanical influences, the precipitate reverts to the room temperature stable monoclinic form.

1. Introduction

Pure zirconia has three polymorphs: the stable room temperature form is monoclinic; on heating to about 1100° C it transforms to a tetragonal structure which on further heating above 2300° C transforms to a fluorite-type cubic structure. The monoclinic–tetragonal phase transition renders the material useless as a high temperature structural ceramic since it is associated with a large volume change which causes cracking and subsequent failure of fabricated products. The phase changes may be suppressed by stabilization of the high temperature cubic fluorite form by alloying with other oxides such as those of magnesium, calcium or yttrium. It is generally accepted however, that the most useful mechanical properties are obtained by partial stabilization so that a two- or three-phase microstructure results. These materials are referred to as partially stabilized zirconias (PSZ).

The improved properties in conventional PSZ materials have been attributed to a fine dispersion of monoclinic phase in a cubic matrix [1, 2]. Prior to recent work by Garvie *et al.* [3] on calcia–PSZ (Ca–PSZ) it was not thought possible to retain the tetragonal phase at room temperature in fabricated and engineering materials, although Lefevre [4] has reported a room temperature tetragonal phase in his study of the zirconia–yttria system at $YO_{1.5}$ contents greater than 4 mol %. Garvie *et al.* [3] showed that in Ca–PSZ, by a rapid cooling and subsequent ageing treatment, tetragonal domains which increased in size with time of ageing were retained at room temperature.

Garvie *et al.* [5] also found that the presence of tetragonal domains strengthened the Ca–PSZ material. It was found that maximum strengthening occurred when the tetragonal domains were of a size where they were critically metastable, i.e. where, at room temperature, they reverted to a monoclinic form upon the application of mechanical stress [5]. This same observation has also been found true for magnesia–PSZ (Mg–PSZ) [6] and yttria–PSZ (Y–PSZ). Porter and Heuer [7] have also reported an improvement in mechanical properties of Mg–PSZ resulting from the dispersion of a tetragonal phase.

The purpose of the present work was to study the growth morphology of the tetragonal phase precipitated in magnesia, calcia and yttria partially stabilized zirconias. Growth mechanisms of the tetragonal phase are analysed in terms of the difference in lattice parameters between the cubic and tetragonal phases.

2. Experimental

2.1. Sample preparation

All samples were prepared by a standard sintering

route. The starting materials were zirconium dioxide powder (99.7% purity, Ugine Kuhlmann glass grade) partially stabilized with oxides of the various stabilizers of >99% purity on calcination. Full details of the powder preparation procedures have been reported elsewhere [8].

Final sample compositions were 9.98 mol % $MgO–ZrO_2$, 8.4 mol % $CaO–ZrO_2$ and 9.74 mol % $YO_{1.5}–ZrO_2$. The samples were sintered and solution-treated in the fluorite phase field at 1800° C using a gas fired furnace. From the sintering temperature to 1300° C the samples were cooled at about 10° C min^{-1}, thereafter at ~50° C h^{-1} to 500° C and then at the natural cooling rate of the furnace to room temperature. Samples in the solution treated and standard cooled condition will be referred to as "as-fired".

Ageing treatments were carried out in air, on 3.2 mm x 3.2 mm x 40 mm bars, using an electrically heated tube furnace. Ageing temperatures used were 1420° C for Mg–PSZ and 1300° C for Ca–PSZ and Y–PSZ. After ageing the bars were furnace-cooled. Corrections to total ageing times for heating and cooling times were generally not necessary as they were short compared with ageing periods used.

2.2. Tetragonal indexing and terminology

The tetragonal phase to be discussed is similar to the primitive tetragonal cell ($P4_2/nmc$) originally reported by Teufer [9]. In this work, to simplify interphase relationships, the tetragonal phase is described in terms of the non-primitive cell referred to in more recent work [4, 10]. This cell has twice the volume of the primitive cell and it is effectively a distorted fluorite structure which can thus be related more readily to the parent cubic fluorite form.

Although interphase interfaces have been studied for some time it is possible that some ambiguity of the term "coherency" could still exist. In the present context the tetragonal domains are considered to remain coherent whilst all lattice planes are continuous across the domain/matrix interface – a small difference between the fluorite and tetragonal lattice parameters and the lack of interfacial dislocation contrast is considered evidence for coherency.

Another possible area of ambiguity is in the definition of the term "habit plane". Habit planes are generally defined as the crystal planes of a matrix which are parallel to the major face of a precipitate. In this work because of the general irregularity in the shape of the domains the habit planes of the fluorite phase were assumed to be those containing the major axes of the domains.

2.3. Electron microscopy

In electron microscopy the geometry of a specific particle or defect is generally found by tilting the specimen to different orientations and then using a stereographic projection to determine the nature of its prominent features. This technique is described as "trace analysis" [11]. For the samples studied here an attempt was made to determine the habit plane of the tetragonal phase. Due to the curved nature and clustering of the domains only the possible habit planes could be determined. These were determined by plotting the projected long axis of domains in Mg–PSZ, the projected edge directions of domains in Ca–PSZ and the directions of domain sheets in Y–PSZ. In all cases

TABLE I Physical parameters of the tetragonal phase in the cubic fluorite matrix, determined from X-ray measurements

Material	Lattice parameter (nm)			Cell volume difference V_t/V_f (%)	c_t/a_t	Angular deviation from planar coincidence $\phi = \tan^{-1}(c_t/a_t) - \pi/4$	Misfit parameter		Calculated maximum coherent boundary length (nm)	
	Cubic	Tetragonal					$\delta_{(a_f-a_t)}$	$\delta_{(a_f-c_t)}$		
	a_f	a_t	c_t						a_t	c_t
Mg–PSZ	0.5080 ± 0.0002	0.5077 ± 0.0002	0.5183 ± 0.0002	+1.947	1.021	1.203°	-0.5×10^{-3}	20.2×10^{-3}	1016	25
Y–PSZ	0.5130 ± 0.0002	0.5116 ± 0.0001	0.5157 ± 0.0001	+0.015	1.008	0.458°	-2.6×10^{-3}	5.4×10^{-3}	197	95
Ca–PSZ	0.5132 ± 0.0001	0.5094 ± 0.0001	0.5180 ± 0.0002	−0.575	1.017	0.974°	-7.5×10^{-3}	9.2×10^{-3}	For {001} habit	
									68	55
									For {110} habit	
									47	40

the same domains were imaged in at least four different fluorite orientations and then their relevant directions plotted. A more comprehensive description of the technique is to be found elsewhere [11, 12].

2.4. X-ray studies

A diffractometer was used to estimate the relative fluorite and tetragonal phase content of unmachined as-fired sintered surfaces. The relative proportion of each phase was determined by comparing the areas under the $4\,0\,0_f$ (fluorite) and $4\,0\,0_t$ and $0\,0\,4_t$ (tetragonal) diffractometer [13].

The room temperature fluorite and tetragonal lattice parameters were determined using a Guinier–Hagg focusing camera. The samples normally used in this camera are powders; these could not be used because in the majority of cases crushing caused the tetragonal phase to revert to the room temperature stable monoclinic form. Thus the X-ray samples used were ion-thinned foils, previously examined in the electron microscope. To facilitate accurate lattice parameter determinations, a thoria standard was deposited on the surface of the foils. When a powder sample could be prepared the thoria was mixed with the powder.

2.5. Misfit parameter and coherent boundary length determination

The strain or misfit parameter, δ, between two lattices is defined by the expression:

$$\delta = \frac{2(a - a_0)}{a + a_0}$$

where a and a_0 are the lattice parameters of the precipitate and matrix respectively [11]. In our case these values are replaced by a_f, a_t and c_t for the various samples. It should be appreciated that δ is a "constrained" misfit parameter since the values of a_t and c_t were determined for the constrained tetragonal phase; it will underestimate the "free" misfit.

The probable extent of domain coherency has been calculated approximately using the simple geometric criterion proposed by Brooks [14]. Brooks suggests that coherency is lost when the total displacement along an interface length, Δd, is equal to the Burgers vector, **b**, of an interfacial dislocation i.e. the domains remain coherent while $\Delta d.\delta < \mathbf{b}$. It is assumed that the Burgers vector will be the same as the lattice vector in the possible habit plane. This model is generally considered to give an underestimate of Δd in most cases [11], nevertheless as a first approximation it serves as a useful criterion to establish the minimum size at which coherency may be lost.

3. Results and observations

3.1. Mg–PSZ

Indexed Guinier–Hagg X-ray photographs from as-fired samples indicated that a fluorite phase was present. Broad $2\,0\,0_f$ and $3\,1\,1_f$ reflections and diffuse intensity around these positions suggested a highly strained phase and that a tetragonal phase was probably also present. Photographs from samples aged for 1 h at 1420° C could be indexed in terms of a two-phase mixture of fluorite and tetragonal. The expected X-ray line intensity ratios from equilibrium fluorite or equilibrium tetragonal structures were not observed in these materials. This observation is discussed in Section 4.1.

X-ray diffractometer traces obtained from the surface of samples aged for 1 to 3 h showed three distinct peaks in the neighbourhood of the $4\,0\,0_f$ reflection. The tetragonal phase content of these surfaces was determined to be $35 \pm 10\%$. The tetragonal content did not alter with ageing time, up to the limit of tetragonal stability, namely 3 h. Ageing beyond 3 h at 1420° C resulted in the appearance of monoclinic reflections.

Within the range of metastability, the lattice parameters for the two phases determined from Guinier–Hagg photographs remained constant and are given in Table I. Some other physical properties, determined from the lattice parameters, are also shown in Table I. Two significant observations are that the cell volume of the tetragonal phase is 1.94% larger than the stabilized fluorite phase and that the calculated maximum coherent boundary length is about forty times larger for the a_t than the c_t direction.

Electron diffraction patterns obtained from as-fired samples showed diffuse banding in addition to the fluorite and tetragonal reflections. Banding of this nature is generally associated with the presence of ordering processes [15, 16]. Examination of electron diffraction patterns from a foil oriented to the $[0\,0\,1]_f$ showed that the $[1\,0\,0]_t$ direction could be parallel to any of the three $\langle 1\,0\,0\rangle_f$ directions and the $(1\,0\,0)_t$ plane could be parallel to any of the three $\{1\,0\,0\}_f$ planes. Due to the large difference between the fluorite parameter and the tetragonal c-axis it was possible to observe the three tetragonal orientation variants in the

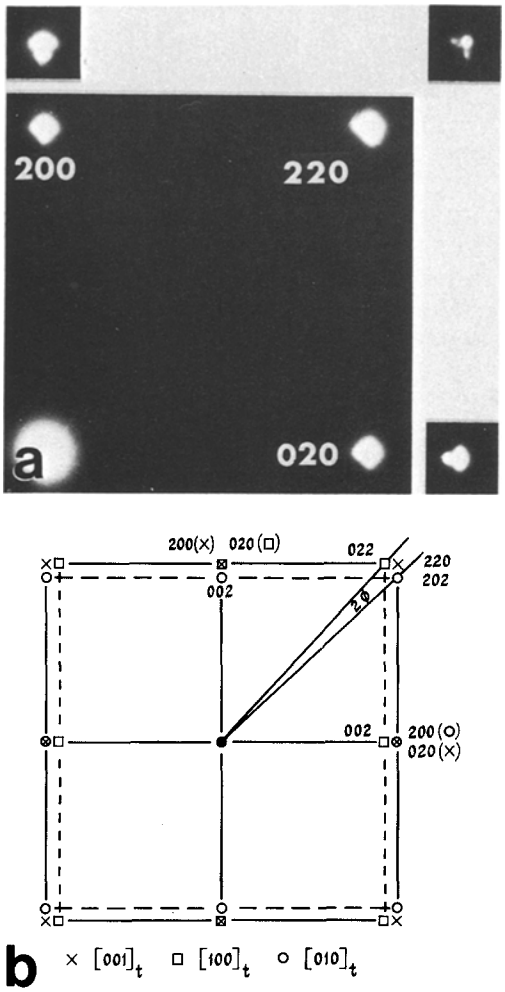

Figure 1 [0 0 1] diffraction pattern of Mg–PSZ. (a) Tetragonal satellites around fluorite reflections, pattern indexed in terms of fluorite. (b) Schematic [0 0 1] pattern indexed in terms of the three tetragonal variants, fluorite reflections omitted.

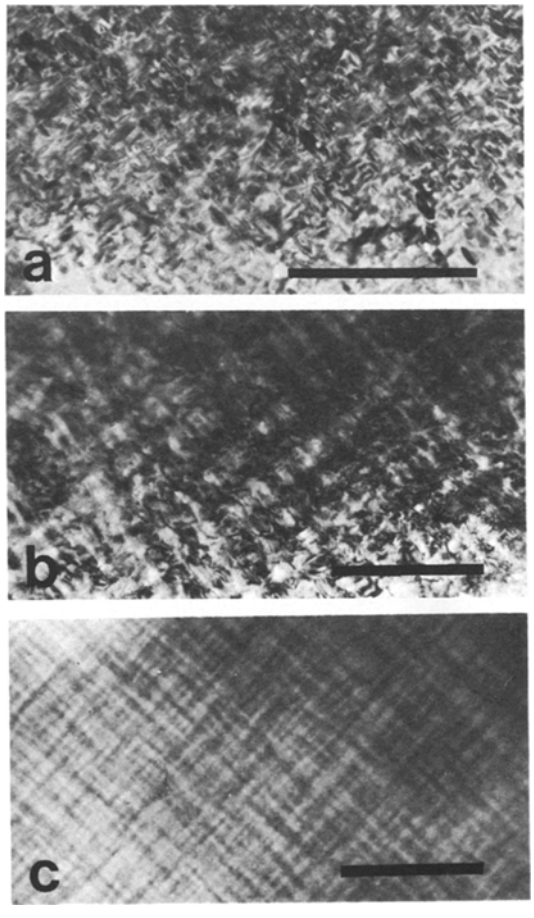

Figure 2 Bright-field transmission electron micrographs from as-fired (a) Mg–PSZ, (b) Ca–PSZ and (c) Y–PSZ, illustrating a highly strained matrix of Mg–PSZ and tweed-like contrast in Ca–PSZ and Y–PSZ. Bars equal 0.5 μm.

electron diffraction patterns. Fig. 1a shows a composite of the tetragonal spots in the $[0\,0\,1]_f$ orientation and Fig. 1b the schematic diffraction pattern indexed in terms of the three variants.

The tetragonality (i.e. the non-unity value of the c/a ratio) of the tetragonal phase will result in a misfit when domains of different variants impinge. This angular deviation from planar coincidence of the impinging domains is defined by 2ϕ and is related to the tetragonality factor by the expression $\phi = \tan^{-1}(c/a) - \pi/4$ [17]. The ϕ value could be measured directly from [1 0 0] oriented electron diffraction patterns such as Fig. 1a. The measured value of $\sim 1.25^\circ$ is in good agreement with the value of $\sim 1.20^\circ$ calculated from X-ray measurements.

As-fired material examined in bright-field illumination showed a highly strained material consisting of a matrix containing small elongated precipitates (see Fig. 2a). Dark-field imaging revealed small ellipsoidal domains, Fig. 3a, whose sizes are given in Table II.

Annealing for 1 h at 1420° C caused considerable domain growth with little domain impingement. The domains appeared to grow with only a limited number of habit variants within any one region. Figs. 4a to c show regions of domains with a common orientation. These figures were obtained by imaging with two different tetragonal reflections, whose intensities were varied by adjusting the Bragg condition to a maximum, alternately to obtain images (a) and (c), and equal for both to obtain (b).

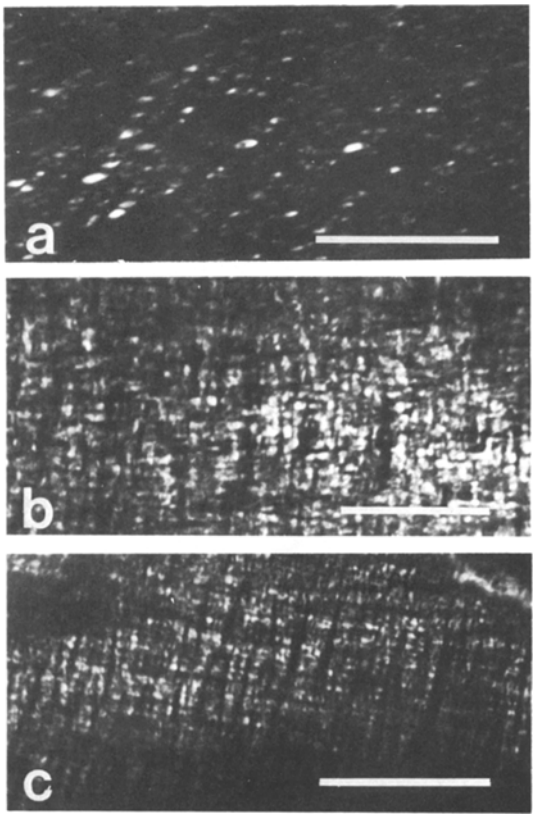

Figure 3 Dark-field transmission electron micrographs from as-fired (a) Mg–PSZ, (b) Ca–PSZ and (c) Y–PSZ showing the tetragonal phase distribution.

TABLE II Observed tetragonal domain sizes

Material	As-fired domain size (nm)	Maximum measured coherent domain size (nm)
Mg–PSZ	36 ± 14	500 ± 85
	11 ± 4	65 ± 25
	< 10 not measured	
Y–PSZ	20 ± 6	not determined but > 100
Ca–PSZ	40 ± 16	90 ± 30

After anealing for 2 h at 1420° C the domains had grown to about 250 nm in the longest direction. As no interfacial dislocation contrast or twinning was observed in the domains they were considered to be still coherent. By examining the same domains in a number of different foil orientations, namely [1 0 1], [2 1 1], [1 1 1], [1 1 2] and another area in [0 0 1], it became evident that the domains were ellipsoidal in shape. This shape was similar to that of the domains described by Porter and Heuer [7] for a 8.1 mol % Mg–PSZ. By plotting the directions of the longest axis of

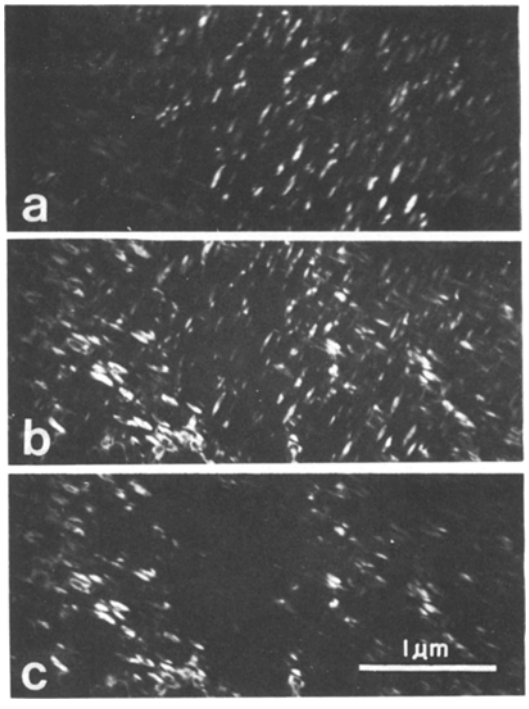

Figure 4 Mg–PSZ aged 1 h at 1420° C showing the preferred alignment in domain sheets, (a) $s < 0$, (b) $s = 0$ and (c) $s > 0$. Dark-field images.

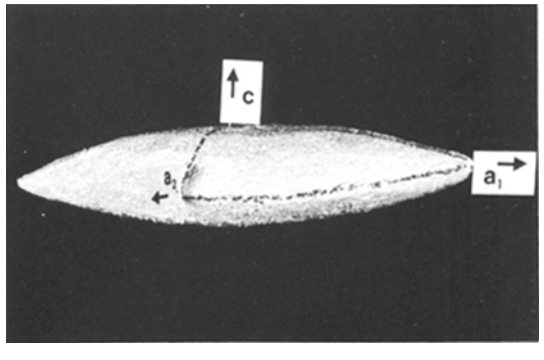

Figure 5 Model of domain morphology in Mg–PSZ aged for 2 h at 1420° C.

each domain observed in the four orientations mentioned above on a stereographic projection, the likely fluorite plane parallel to the longest axis, i.e. the habit plane, was found to be $\{1\,0\,0\}_f$. Using a tetragonal reflection from a split high order $h\,0\,0_{f,t}$ reflection to form a dark-field image, the *c*-axis direction within the domain could be unambiguously determined. This direction was found to lie parallel to the shortest measured domain dimension. Combining these data with the habit plane and measuring domain dimensions in a $[1\,0\,1]_f$ orientation (correcting for angles in the foil) resulted in determination of ratios of ~2.5

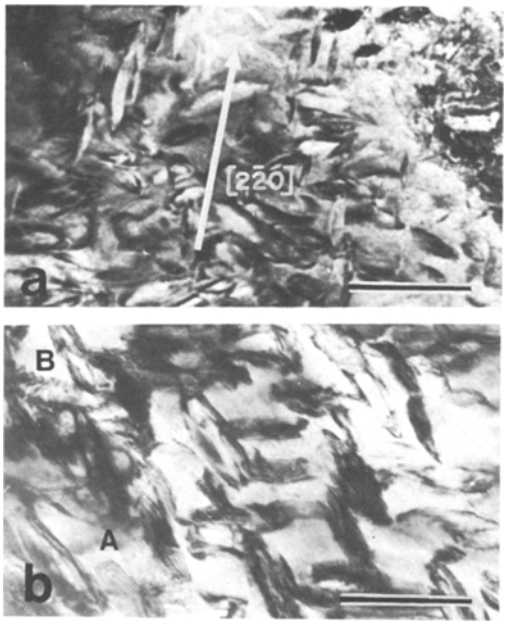

Figure 6 (a) Mg–PSZ aged 2 h at 1420° C, foil normal [1 1 0], domains along [2 $\bar{2}$ 0] have *c*-axes parallel to beam, whilst the other two variants are at 45°. (b) Mg–PSZ aged 6 h at 1420° C, tetragonal domains showing coherency fringes (A) whilst domains transformed to monoclinic have twinned (B). Note also tetragonal domains attaining a "rhombic or lozenge" shape. Bright-field images; bar length 0.5 μm.

for the two largest axes and ~5.5 for the longest axis with respect to the shortest axis, i.e. the *c*-axis (cf. the domains in Fig. 6a). A model of the ellipsoidal domain morphology based on these aspect ratios is shown in Fig. 5.

In samples ages for 4 h, in addition to the ellipsoidal domains previously observed, some tetragonal domains, when examined in $[0\,0\,1]_f$ orientations, exhibited lenticular and rhombic shapes. The coherency fringe contrast observed in the rhombic domains suggested that the domains were becoming plates, the edges acquiring a straighter profile with the longest edge preferring $[2\,1\,0]_f$. After ageing for 6 h at 1420° C domains which remained tetragonal had grown to ~600 nm in the longest *a*-axis direction (Fig. 6b).

3.2. Ca–PSZ

X-ray films of as-fired material could be indexed in terms of a tetragonal structure only i.e. the $2\,0\,0_f$ and $3\,1\,1_f$ reflections were not observed. Ageing for 20 h at 1300° C developed the $2\,0\,0_f$ and $3\,1\,1_f$ reflections. Ageing periods longer than 56 h caused the appearance of weak diffuse monoclinic reflections. The fluorite and tetragonal lattice parameters and tetragonal domain characteristics derived from these measurements are shown in Table I. X-ray diffractometer traces, from samples where the two phases were present, showed about 55% tetragonal content. This content did not alter until the appearance of the monoclinic phase.

Electron diffraction patterns of as-fired materials showed diffuse banding similar to those arising from the ϕ_1-phase ($CaZr_4O_9$) observed by Allpress and Rossell [15]. The fluorite and tetragonal orientation relationships were the same as those observed for Mg–PSZ.

Bright-field images of as-fired materials showed the presence of a "tweed-like" contrast (see Fig. 2b). The tweed-like contrast results from the alignment of tetragonal domains in a fluorite matrix. The tweed spacing was ~70 nm. Dark-field imaging revealed small equiaxed domains aligned in a modulated or wavy pattern, see Fig. 3b.

Ageing periods up to 64 h at 1300° C caused domain growth and an associated coarsening of the modulated structure – the domain sizes are given in Table II. By examining domains in a number of different orientations it was concluded a variety of domain morphologies were present. These included cubes, irregular rectangular plates and an irregular equiaxed form. The edges of the regular domains preferred $\langle 1\,1\,0\rangle_f$, as shown in Fig. 7.

A determination of the habit plane was made by plotting the observed edge directions, for a number of the same equiaxed domains, observed in several different beam directions. This procedure showed that the domains prefer habit planes close to $\{1\,1\,0\}_f$. Due to the curved nature of the edges a more accurate determination was not possible.

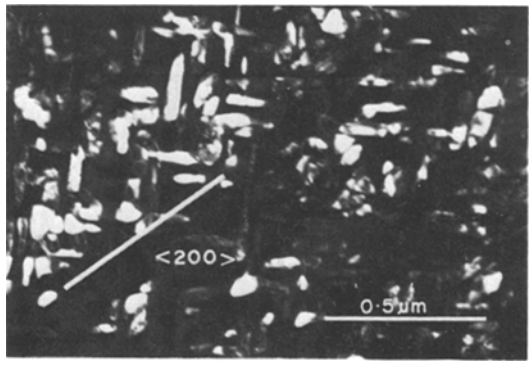

Figure 7 Tetragonal domain morphology in Ca–PSZ aged for 64 h at 1300° C. Dark-field image; the electron beam direction was close to [0 1 2].

3.3. Y–PSZ

As with Ca–PSZ X-ray films obtained using as-fired samples could be indexed in terms of the tetragonal phase only. Ageing for 100 h at 1300° C failed to develop the $3\,1\,1_f$ reflections, although crushing this sample resulted in the appearance of $3\,1\,1_f$ between diffuse $1\,1\,3_t$ and $3\,1\,1_t$ reflections. Unlike the other materials studied here, crushing did not result in the appearance of the room-temperature stable monoclinic phase. A consequence of crushing was a significant change in the tetragonal parameter, from 0.5116 ± 0.0001 nm to 0.5103 ± 0.0001 nm.

Electron microscopy showed the presence of the fluorite phase so that, for as-fired and 100 h aged samples, the a_f parameter was deduced from fluorite reflections which coincided with tetragonal reflections, and which did not appear when the sample was crushed, namely the 1 1 1, 2 0 0, 2 2 0 and 2 2 2 reflections. The lattice parameters obtained by this selection process are in good agreement with the values measured by Lefevre [4] for homogeneous single phase samples of this same composition; this is probably an indication of a non-equilibrium phase composition and/or the highly strained nature of the two phases present. The parameters and domain characteristics are presented in Table I.

In diffractometer traces the $4\,0\,0_f$ peak could not be resolved from the $4\,0\,0_t$ and $0\,0\,4_t$ peaks so that the tetragonal content could not be determined.

Bright-field electron microscope images showed tweed-like contrast (see Fig. 2c) similar to Ca–PSZ. In this case the contrast was also the result of domain alignment and the tweed spacing was ~55 nm. As with Ca–PSZ, dark-field images showed the projected domains to be nearly equiaxed and arranged in a modulated or wavy pattern, Fig. 3c. The domain sizes are shown in Table II.

Ageing for 100 h at 1300° C resulted in domain coarsening and impingement. The domain clusters in the as-fired material became more clearly defined as large rectangular plate-like agglomerates about 30 nm by 100 nm and about one domain thick, see Fig. 8. The spacing between the sheets had increased to approximately 65 nm.

Only the long edges of the domain sheets could be plotted in an effort to determine their habit plane, because the sheets did not possess straight ends. As an unambiguous determination was not possible only the "likely" habit plane can be stated. This was considered to be a low order plane in the zone defined by the direction of the sheet edge. The lowest order plane in this zone was a $\{1\,0\,0\}_f$, although on the basis of measurement accuracy the $\{1\,1\,0\}_f$ could not be ruled out. The long axis of the sheets preferred to lie along approximately $\langle 0\,0\,1\rangle_f$. Because domain growth was sluggish the domains were not aged to a size where they would be expected to lose coherency.

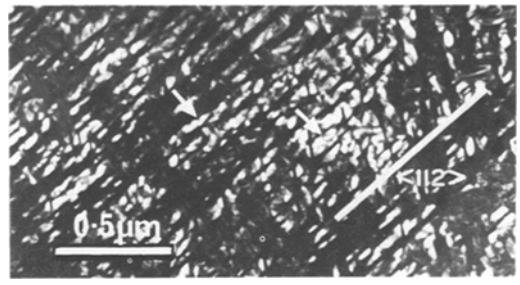

Figure 8 Tetragonal domain distribution and morphology in Y–PSZ aged for 100 h at 1300° C, illustrating domain clustering and domain impingement separated by anti-phase boundaries (arrowed) in dark-field image. The electron beam direction was close to $[1\,1\,\bar{1}]$.

4. Discussion

4.1. X-ray measurements

The lattice parameter measurements indicate that, for the ageing times used, cation segregation subsequent to that observed in as-fired material did not occur to a measurable extent. This observation was also supported by determination of the tetragonal content, made from diffractometer peaks of aged Mg–PSZ and Ca–PSZ materials, which showed that up to the limit of tetragonal stability the content remained constant. Therefore, for the cooling rate employed, nucleation and precipitation of the tetragonal phase was complete on cooling from the firing temperature, and subsequent ageing treatments only resulted in coarsening the precipitates.

X-ray line broadening data and the bright-field electron microscope images suggested that the materials were highly strained, so that the lattice parameters measured would not be equilibrium values. Significant lattice parameter differences between the three PSZ materials were observed. These differences, seen in Table I, were basically a function of the size of stabilizer cation used and the resultant tetragonal cell volumes were both larger and smaller than the fluorite cell volume.

As mentioned in Section 3.1, the X-ray line

intensity ratios expected for equilibrium cubic fluorite and tetragonal structures were not observed. The departures may be due to the lattice strain and the size and morphology of the tetragonal phase. The reason for the apparent absence of certain fluorite reflections, such as 2 2 0 and 3 1 1, in Guinier-type photographs obtained from the as-fired samples is not known. One plausible explanation is presented. In the Ca–PSZ and Y–PSZ as-fired samples, the X-ray patterns were indexed as tetragonal. It was seen from the electron microscope observations, however, that the cubic phase was also present and that the distance between the domains, R, was small compared with the domain size, r. Tanner [17] has deduced from the work of Eshelby [18] that the strains surrounding a coherent particle fall off with the reciprocal of the distance cubed. Hence the effect of tetragonal distortion will be greatest close to the coherent interface. When the distance between the domains is small compared with their size, the strain fields will overlap and the fluorite matrix can be distorted to give diffuse reflections around the tetragonal positions. As the domains grow the distance between them increases; the fluorite is on average less strained and fluorite reflections will appear. In Mg–PSZ, where X-ray diffraction patterns from as-fired samples appeared to indicate the materials was basically fluorite, electron microscopy showed $R > r$. The close values of a_f and a_t combined with the small amount of growth in the tetragonal c-axis direction probably results in the c-axis parameter being distorted to the fluorite value so that highly diffuse reflections result. Thus the as-fired Mg–PSZ sample showed a mixture of fluorite and unresolved tetragonal.

4.2. Nucleation morphology

Eshelby [18], as interpreted in [17], has shown that the strains associated with a transformation will determine the shape of coherent nuclei in order to attain the lowest strain energy. For cubic to tetragonal transformations, as in this case, flat disk-shaped particles have the lowest strain energy. Due to the speed of reaction and the cooling rates used in this work, the initial shape of the tetragonal phase could not be studied. However in other work on Ca–PSZ carried out in this laboratory (Stringer *et al.*, unpublished), samples water quenched from 1900° C contained small randomly distributed spherical and disk-shaped tetragonal precipitates. This observation agrees with the work of Warlimont [19], which shows that if the misfit is small ($\delta < 0.01$) the precipitates are initially spherical and the array is random.

At the stage in thermal history where the observations in this work commenced, the Mg–PSZ material contained randomly dispersed ellipsoid-shaped domains while in the Ca–PSZ and Y–PSZ samples the precipitates were equiaxed or spherical and appeared as closely spaced bands. A consequence of the closely spaced domains and their preferred alignment is the presence of the "tweed-like" contrast observed in the electron microscope [17, 20].

4.3. Growth morphology

The growth process of the tetragonal domains with the different stabilizers will be considered individually in terms of their misfit parameter. Another factor is that the elastic anisotropy of zirconia, which is unknown, may be large [21] as it is for thoria. If so it will play a significant part in the final tetragonal phase distribution and morphology.

If the growth of the domains is limited by interfacial strain, the observed final morphology will be a function of the mismatch parameter. The strain field interaction coupled with the elastic anisotropy will control the final distribution of the domains in a manner similar to that observed in aged Ni–Al alloys [20], where it was shown that there existed an elastic interaction between precipitated particles arising from the difference between the elastic moduli in the precipitate and matrix.

The curvature of the domain surface approximately normal to the tetragonal c-axis in Mg–PSZ (see Fig. 5) can be explained in terms of surface mismatch strains which are kept to a minimum as the a-axis grows. Lattice parameter measurements have shown $a_t = a_f$ and that the c-axis mismatch is about forty times larger than that of the a-axis. This large difference in mismatch results in an almost classical tetragonal precipitate morphology, i.e. a disk. Probably due to the speed of nucleation and growth the a-axis directions initially grow so rapidly that an ellipsoid results, the edges of ellipsoids being formed by coherent ledges. Individual monatomic ledges are not readily visible by strain contrast because the misfit in this case is too small [22]. With longer ageing times the c-axis mismatch begins to dominate and the domain either loses coherency or further growth occurs predominantly by growth and ledge migration parallel to the a-axis.

This final growth process results in the rhombic-shaped platelets seen in Fig. 6b. A similar nucleation and growth process has been observed by Tanner in Ni_2V alloys [23], where homogeneously nucleated particles grow initially as faceted ellipsoids and, given sufficient time, become elongated parallelepipeds. Another feature of the domains in Mg–PSZ is that growth is initially much faster in one of the a-axes directions. This preferential growth may occur when an a-axis grows into the strain field of the c-axis of another domain allowing the variants to impinge at their edges.

The cuboid or fairly equiaxed morphologies observed in Ca–PSZ are consistent with the X-ray measurements, which indicate that δ is about equal in the a_t and c_t directions, see Table I. The almost equal differences, $|a_f - a_t|$ and $|a_f - c_t|$ would then result in equal probability for domain growth along all axes. The final tetragonal domain shape, at 90 nm, would then be controlled by the interacting strain fields. The final morphologies near the limit of coherency are shown in Fig. 7.

In Y–PSZ where δ was twice as large along the tetragonal c-axis as along the a-axis, the domains showed no preference for circular disks. Instead, fairly irregular domains clustered in a plate-like alignment with the long plate axis approximately parallel to ⟨0 0 1⟩.

Using the Brooks [14] analysis to determine the possible extent of the coherent boundary, it was found that for Mg–PSZ the domain coherency would be limited by the c-axis length to about 25 nm. In Ca–PSZ the calculated length was ~40 nm, whilst for Y–PSZ domain boundary lengths of ~100 nm were the limit. Considering the Brooks criterion as being an underestimate of the calculated boundary length [11] then, on the basis of the maximum expected coherent boundary length and the maximum measured tetragonal domain size, one aspect of the tetragonal–monoclinic transformation becomes apparent. Since the interfacial misfit in these materials could be accommodated by one dislocation it suggests that the domains transform to monoclinic form, on cooling, when coherency of an interface is lost. This aspect of the tetragonal–monoclinic transformation in Ca–PSZ and its implications to a possible strengthening mechanism are discussed in another paper [13].

5. Summary and conclusions

(1) X-ray measurements, of electron microscope foils, showed that the cubic fluorite and tetragonal lattice parameters of the various samples remained effectively constant for all thermal treatments employed here. This observation suggested that precipitation of the coherent tetragonal phase was virtually completed during the initial fast furnace cool from 1800° C; subsequent ageing merely coarsened the scale of the precipitates.

(2) The volume of the tetragonal cell in Mg–PSZ was larger, that of Ca–PSZ was smaller, whilst that of Y–PSZ was almost identical to the volume of the cubic fluorite cell.

(3) The specific mode of nucleation could not be stated, but the precipitate distribution was similar to that expected from a system undergoing a homogeneous nucleation and precipitation process.

(4) The limiting size and morphology of the tetragonal domains was different in each of the systems studied. For the ellipsoid-shaped domains in Mg–PSZ the coherency limit of about 25 nm was controlled by growth of the domain in the tetragonal c-axis direction, although lengths parallel to the tetragonal a-axis of about 600 nm have been observed. The domains in Ca–PSZ varied from cuboids and rectangular plates to irregular equiaxed forms whose longest coherent dimension was about 90 nm. Y–PSZ domains agglomerated into plates about 100 nm long by 60 nm wide and one domain (~25 nm) thick. These differences in size and morphology between the various samples can be approximately explained in terms of the misfit between the tetragonal and cubic structures.

(5) Habit planes for growth of the tetragonal domains in Mg–PSZ were {1 0 0} with preferred alignment of the long domain axis close to ⟨0 0 1⟩. The possible habit planes for the tetragonal domains in Ca–PSZ were {1 1 0} and the domain sheets in Y–PSZ preferred alignment along approximately ⟨0 0 1⟩.

(6) It was found for Mg–PSZ and Ca–PSZ that when domains had grown to a size where interfacial coherency was lost the domains transformed, on cooling, to the room temperature stable monoclinic form.

Acknowledgements

The author takes pleasure in acknowleding the assistance of Mr C. Urbani for preparing the original samples. The author also wishes to thank his colleagues, in particular Dr K. A. Johnston, Dr H. G. Scott and the late Dr R. T. Pascoe, for their friendly discussion and constructive criticism of the work.

References

1. R. C. GARVIE and P. S. NICHOLSON, *J. Amer. Ceram. Soc.* **55** (1972) 152.
2. G. BANSAL and A. H. HEUER, *ibid.* **58** (1975) 235.
3. R. C. GARVIE, R. H. J. HANNINK and R. T. PASCOE, *Nature* **258** (1975) 703.
4. J. LEFEVRE, *Ann. Chim.* 8 (1963) 117.
5. R. C. GARVIE, R. H. J. HANNINK, R. R. HUGHAN, N. A. McKINNON, R. T. PASCOE and R. K. STRINGER, *J. Aust. Ceram. Soc.* **13** (1977) 8.
6. R. T. PASCOE, R. H. J. HANNINK and R. C. GARVIE, "Science of Ceramics", Vol. 9, Noordwijkerhout (European Ceramic Society, The Netherlands, 1977).
7. D. L. PORTER and A. H. HEUER, *J. Amer. Ceram. Soc.* **60** (1977) 183.
8. R. C. GARVIE, R. R. HUGHAN and R. T. PASCOE, Processing of Crystalline Ceramics (Conference, Raleigh, USA, 1977).
9. G. TEUFER, *Acta Cryst.* **15** (1962) 1187.
10. O. RUFF and F. EBERT, *Z. Anorg. Chem.* **180** (1929) 19.
11. P. B. HIRSCH, A. HOWIE, R. B. NICHOLSON, D. W. PASHLEY and M. J. WHELAN, "Electron Microscopy of Thin Crystals" (Butterworths, London, 1965) Ch. 14.
12. A. K. HEAD, P. HUMBLE, L. M. CLAREBROUGH, A. J. MORTON and C. T. FORWOOD, "Computed Electron Micrographs and Defect Identification" (North-Holland, Amsterdam, 1973) Ch. 3.
13. R. H. J. HANNINK, K. A. JOHNSTON and R. T. PASCOE, *J. Mater. Sci.* (submitted).
14. H. BROOKS, "Metal Interfaces" (American Society for Metals, Cleveland, 1952) p. 20.
15. J. M. COWLEY, *Acta Cryst.* **A29** (1973) 537.
16. J. G. ALLPRESS and H. J. ROSSELL, *J. Solid State Chem.* **15** (1975) 68.
17. L. E. TANNER, *Phys. Stat. Sol.* **30** (1968) 685.
18. J. D. ESHELBY, *Proc. Roy. Soc.* **A241** (1957) 376.
19. H. WARLIMONT, "Electron Microscopy and Structure of Materials," edited by G. Thomas (Berkeley, University of California, 1972) p. 505.
20. A. J. ARDELL and R. B. NICHOLSON, *Acta Met.* **14** (1966) 1295.
21. C. T. FORWOOD and J. G. ALLPRESS, *Crystal Lattice Defects* **5** (1974) 223.
22. G. C. WEATHERLY, *Acta Met.* **19** (1971) 181.
23. L. E. TANNER, *ibid.* **20** (1972) 1197.

Received 8 February and accepted 18 April 1978.